Vol. 483: 19–29, 2013
doi: 10.3354/meps10223

MARINE ECOLOGY PROGRESS SERIES
Mar Ecol Prog Ser

Published May 30

Impact of Typhoon Morakot on chlorophyll *a* distribution on the inner shelf of the East China Sea

Yunhai Li[1,*], Xiang Ye[1], Aijun Wang[1], Haidong Li[1,2], Jian Chen[1], Lei Qiao[3,4]

[1]Third Institute of Oceanography, State Oceanic Administration, Xiamen 361005, PR China
[2]College of Earth Sciences, Jilin University, Changchun 130061, PR China
[3]Hydrometeorology and Remote Sensing Laboratory, University of Oklahoma, Norman, Oklahoma 73019, USA
[4]Atmospheric Radar Research Center, University of Oklahoma, Norman, Oklahoma 73072, USA

ABSTRACT: To study typhoon-induced variations in chlorophyll *a* (chl *a*) distribution, 2 surveys were conducted on the inner shelf of the East China Sea, and 3 remote sensing images were selected before and after the passage of Typhoon Morakot. Chl *a* was predominantly present in coastal waters and the euphotic zone during normal, pre-typhoon conditions at a concentration >0.7 mg m^{-3}. After the passage of the typhoon, the chl *a* concentration drastically declined to <0.5 mg m^{-3}, except for in the surface layer in coastal areas, where the concentration of chl *a* was >1.0 mg m^{-3} due to the abundant fresh water supply from typhoon-induced runoff. Remote sensing data indicated that under normal conditions, the concentration of surface chl *a* was ~1.0 mg m^{-3}, whereas it increased to >10.0 mg m^{-3} post-typhoon. A typhoon-initiated chl *a* increase showed a delay of ~4 to 7 d. A 3-stage conceptual model is proposed to describe the time-evolution of chl *a*. The first stage is the normal, pre-typhoon condition. The second stage is the typhoon-active period, when chl *a* generally decreases due to the presence of opposing factors, such as increasing turbidity and cloud cover, while in the coastal surface water layer, chl *a* is increased due to the fresh water supply. The third stage is the post-typhoon condition, when the opposing factors disappear and an increase in nutrient supply causes an increase in chl *a*.

KEY WORDS: Typhoons · Morakot · Chlorophyll *a* · East China Sea · Field observation · Remote sensing

INTRODUCTION

The course of a typhoon may, on a short time scale, profoundly alter the oceanic water structure (Price 1981, Dickey et al. 1998, Lin et al. 2003, Li et al. 2012), seafloor topography and coastal landforms (Milliman et al. 2007), particle transport (Chang et al. 2001, Bian et al. 2010, Liu et al. 2011), nutrient distribution (Goñi et al. 2006, Herbeck et al. 2011), marine organisms and primary production (Byju & Kumar 2011) in the affected marine area. A typhoon triggers the sequential events of water vertical mixing and upwelling, which can pump nutrient-rich deep water up to the euphotic layer at the sea surface and augment the dissolved oxygen level (Shiah et al. 2000, Chen et al. 2003, Walker et al. 2005, Li et al. 2007, Eliot & Pattiaratchi 2010, Rao et al. 2010). The intense precipitation brought about by a typhoon is able to significantly boost material flux (e.g. fresh water, particles and nutrients) in coastal areas (McKinnon et al. 2003, Zheng & Tang 2007, Herbeck et al. 2011). These processes promote the robust growth of phytoplankton and elevate marine primary productivity, thereby affecting material cycles in the ocean (e.g. the carbon cycle). As such, typhoon processes are not only associated with ferocious wind and waves but are also associated with marine plankton blooms (Lin et al. 2003, Babin et al. 2004, Walker et al. 2005, Zheng & Tang 2007).

*Email: liyunhai1980@gmail.com

Due to the insufficient ability to forecast typhoon events and the difficulties of shipboard operation under severe weather conditions, direct observation is a formidable task. Remote sensing satellites provide unique advantages in typhoon studies by revealing the ocean physical processes, material transport and biogeochemical cycles occurring during a typhoon event (Lin et al. 2003, Babin et al. 2004, Liu et al. 2009, Zheng et al. 2010, Huang et al. 2011). This technique has led to impressive achievements in examining the influence of typhoon processes on chl *a* distribution and the subsequent effects on primary productivity. For example, an investigation of remote sensing data in the South China Sea showed that typhoons may increase chl *a* concentration up to 30-fold, which was estimated to yield a marked augmentation of primary productivity (20 to 30% annually; Lin et al. 2003). Statistical analyses on 4 yr of remote sensing data revealed that typhoon-initiated chl *a* elevation may be sustained for 2 to 3 wk (Babin et al. 2004), which agrees with the estimated impact on marine primary productivity and the carbon cycle (Byju & Kumar 2011). Similar results were also found in other marine areas (Davis & Yan 2004, Zheng & Tang 2007, Huang et al. 2011). However, given that optical remote sensing can only be conducted through little or no cloud cover, it is a great challenge to apply it during typhoon events. In addition, remote sensing can only detect the distribution and evolution of chl *a* concentration at the sea surface and is unable to reach the lower boundary of the thermocline, where chl *a* (phytoplankton) peaks (Suchint & Puntip 2000). Because of the adverse conditions during typhoon events, marine observation is generally performed through moorings, which restricts the location and range of observation (Dickey et al. 1998). Typhoon processes generate broad and lasting influences on the ocean environment. Hence, field surveys immediately after typhoon events, as soon as sea conditions are acceptable, can not only reliably indicate the direct typhoon effects but also compensate for the drawbacks of moored observation. Moreover, the combination of post-typhoon surveys with remote sensing may reflect typhoon influences more comprehensively.

On 1 and 12 August 2009, surveys in the Zhejiang-Fujian coastal mud area on the inner shelf of the East China Sea (ECS) were conducted. The second survey was performed in the study zone where Typhoon Morakot had landed 2.5 d prior to the sampling. In addition, 3 d remote sensing images of sea surface temperature (SST) and surface chl *a* distributions were selected from before and after the typhoon. The differences in chl *a* distribution before and after the typhoon were reviewed and analyzed in conjunction with water temperature, salinity and turbidity data that were generated through field measurements (for detailed information regarding the water column structure in the 2 survey areas, see Li et al. 2012). The distribution of SST, which was derived from the remote sensing data, was also used in these analyses. Our analyses enabled us to evaluate the response of chl *a* distribution to Typhoon Morakot, probe the temporal lag of the typhoon effect and, finally, propose an evolution model of chl *a* distribution in the near-shore area under the influence of a typhoon.

BACKGROUND

Study area and surveys

The study area is located in the mud deposition center off the Zhejiang-Fujian coast, which acts as a sink for Yangtze (Changjiang) River particles and accounts for the primary mud deposits on the ECS inner shelf (Hu & Yang 2001, Liu et al. 2006, 2007, Xu et al. 2012). Sedimentary processes, which are controlled by material supply and marine hydrodynamics, vary seasonally in the mud deposition center (Liu et al. 2006, Xu et al. 2012). The circulation system in the mud deposition center includes the coastal current, which flows northward in summer and southward in winter due to monsoons and has a relatively low temperature, low salinity and high turbidity, and the Taiwan Warm Current (TWC), which perennially flows northward and has a high temperature, high salinity and low turbidity (Su 2005). The particles discharged from the Yangtze (Changjiang) River are obstructed by the northward monsoon and the marine circulations and are generally rapidly deposited in the estuary in the summer (Hu & Yang 2001, Liu et al. 2006, Xu et al. 2012). The deposited sediments can be resuspended by extreme storms and transported southward again along the coast in the winter (Liu et al. 2006). The sediment transport and deposition along the ECS coast primarily occurs in the winter and forms the thickened Zhejiang-Fujian mud wedge (Liu et al. 2006, Xu et al. 2012). According to long-term records, on average, 4 typhoons pass over the ECS shelf annually (Su 2005), which significantly impacts the modern sedimentary environment, including the evolution of biogeochemical cycles.

Two surveys were conducted at the mud deposition center study area (Fig. 1, Table 1). The first survey was conducted on 1 August 2009, followed by a sec-

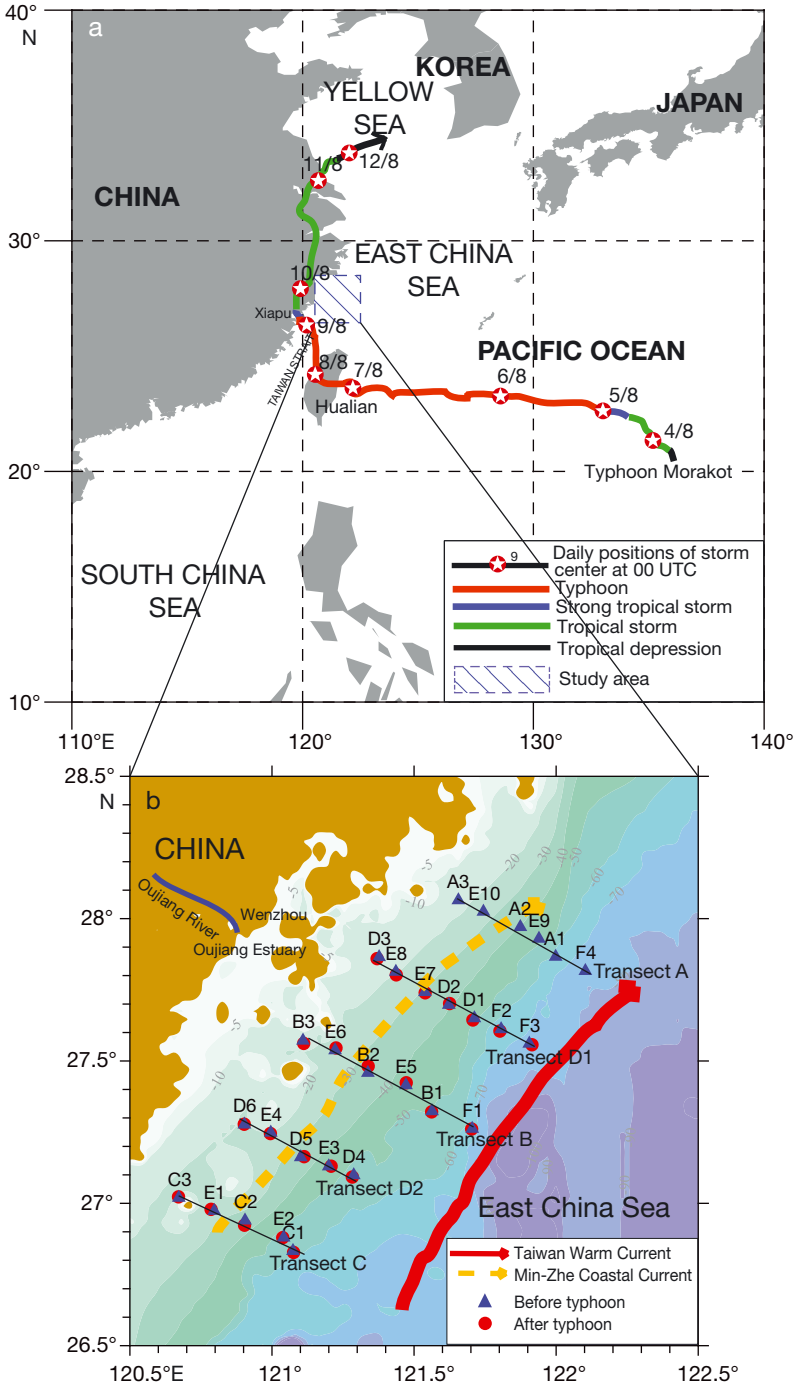

Fig. 1. (a) The track of Typhoon Morakot in August 2009 (modified from the typhoon track data at http://map.weather.gov.cn/). (b) Station locations and survey transects

ond survey on 12 August 2009, which was 2.5 d after Typhoon Morakot made landfall in Fujian on 9 August 2009. The first survey lasted from 1 to 3 August, and data were collected at 29 stations in 5 east–west swaths (labeled as Transects A, D1, B, D2 and C in Fig. 1b). During the first survey, the weather was calm, with southern wind speeds of <10.7 m s^{-1} and wave height <1.6 m (Ocean Monitoring and Forecasting Center of Zhejiang Providence, www.zjhy.net.cn). The second survey lasted from 12 to 14 August, and data were collected at 23 stations in 4 east–west swaths (labeled as Transects D1, B, D2 and C in Fig. 1b). During the second survey, the weather was unfavorable because of the typhoon, with wave heights of 2.0 to 2.5 m and wind speeds >13.0 m s^{-1} (Ocean Monitoring and Forecasting Center of Zhejiang Providence, www.zjhy.net.cn). As our cruise moved northward, the sea conditions deteriorated considerably such that we were forced to abandon the survey for the northernmost portion of Transect A. The 2 surveys represent a normal, pre-typhoon condition and a directly typhoon-affected condition (i.e. the typhoon-active period condition), respectively.

Typhoon Morakot

Typhoon Morakot is the deadliest typhoon to have impacted Taiwan in recorded history, and its name was retired by the World Meteorological Organization. The typhoon was formed early on 2 August 2009 as a tropical depression, which gradually developed into a tropical storm and was named Morakot on 3 August. The large system gradually intensified as it moved westward, toward Taiwan, and by 5 August, Morakot attained typhoon status. Early on 7 August, the typhoon reached its peak intensity with winds of 41.7 m s^{-1} and became the equivalent of a Category 1 hurricane on the Saffir-Simpson hurricane scale. Morakot weakened slightly before making landfall in central Taiwan later that day. The storm re-emerged over the water into the Taiwan Strait on 8 August and weakened to a severe tropical storm before making landfall in mainland China on 9 August. The wind speed was ~33.0 m s^{-1} in Fujian, which is 100 km away from the center of the study area. However, the typhoon reached wind speeds

Table 1. Station locations, depth and times of observations in 2 surveys, where the times of observations were represented as month-day-hour-minute (m-d-h-m). –: no observation

Stn	First survey				Second survey			
	Latitude (°N)	Longitude (°E)	Time (m-d-h-m)	Depth (m)	Latitude (°N)	Longitude (°E)	Time (m-d-h-m)	Depth (m)
A1	27.87	122.00	08-02-17-30	61.2	–	–	–	–
A2	27.97	121.87	08-02-19-41	44.0	–	–	–	–
A3	28.06	121.66	08-02-22-24	21.2	–	–	–	–
B1	27.32	121.56	08-02-05-19	56.8	27.32	121.56	08-13-03-28	50.7
B2	27.46	121.34	08-03-06-41	38.7	27.48	121.34	08-13-00-44	38.2
B3	27.57	121.11	08-03-09-35	21.3	27.56	121.11	08-13-18-56	19.0
C1	26.83	121.07	08-01-18-53	61.2	26.83	121.08	08-12-14-19	61.5
C2	26.94	120.91	08-01-15-05	43.4	26.92	120.90	08-12-11-41	44.1
C3	27.02	120.67	08-01-12-27	19.4	27.02	120.67	08-12-09-12	27.2
D1	27.65	121.71	08-02-10-50	49.4	27.64	121.71	08-13-10-14	49.9
D2	27.70	121.62	08-02-09-43	40.4	27.70	121.62	08-13-11-14	40.7
D3	27.86	121.38	08-03-01-16	17.3	27.86	121.37	08-13-14-05	19.7
D4	27.10	121.29	08-02-00-15	53.9	27.09	121.28	08-12-16-45	48.7
D5	27.16	121.10	08-01-22-05	41.7	27.16	121.11	08-12-19-02	39.9
D6	27.28	120.90	08-03-13-48	23.8	27.28	120.90	08-12-21-15	24.6
E1	26.97	120.80	08-01-13-55	37.0	26.98	120.79	08-12-10-32	37.1
E2	26.88	121.04	08-01-16-39	53.2	26.88	121.04	08-12-13-18	56.4
E3	27.13	121.20	08-01-23-13	47.4	27.13	121.21	08-12-17-57	45.1
E4	27.25	121.00	08-03-12-29	18.2	27.25	120.99	08-12-20-22	30.5
E5	27.42	121.47	08-02-07-01	47.9	27.42	121.47	08-13-02-11	43.5
E6	27.54	121.22	08-03-08-24	28.1	27.55	121.23	08-13-17-45	25.8
E7	27.74	121.54	08-03-03-40	29.0	27.74	121.54	08-13-12-11	33.7
E8	27.81	121.44	08-03-02-22	22.9	27.80	121.44	08-13-13-13	25.8
E9	27.93	121.94	08-02-18-43	52.1	–	–	–	–
E10	28.02	121.74	08-02-21-21	28.7	–	–	–	–
F1	27.26	121.70	08-02-03-49	70.5	27.26	121.70	08-13-05-01	60.0
F2	27.61	121.81	08-02-12-02	62.9	27.61	121.80	08-13-09-07	62.7
F3	27.56	121.91	08-02-13-13	75.1	27.56	121.91	08-13-07-37	75.3
F4	27.82	122.10	08-02-16-08	68.7	–	–	–	–

>40.0 m s^{-1} over the sea. Subsequently, Morakot migrated along the Zhejiang-Shanghai-Jiangsu coast in eastern China. On 12 August, Morakot entered the southern Yellow Sea and weakened into a tropical depression, which marked the end of its influence. The storm produced copious amounts of rainfall, peaking at 2777 mm and surpassing the previous record of 1736 mm, which was set by Typhoon Herb in 1996. During 4 d of lingering, Morakot produced up to 1240 mm of rain in Zhejiang province, which was the highest in nearly 60 yr in the province, raising several rivers above their flood stages (NMCCMA 2009).

Water structure variations due to Typhoon Morakot

According to a previous study result, water temperature, salinity and turbidity distributions were greatly different in 2 surveys before and after Typhoon Morakot (Li et al. 2012) (Fig. 2). After the passage of the typhoon, the water column was mixed more thoroughly. The stratification and thermocline were interrupted. Water temperature increased in the lower layer and decreased in the upper layer. Meanwhile, due to vertical water mixing and the abundance of fresh water supply, salinity decreased on average. Low-salinity water spreading in the upper layer produced a halocline near the coastal area. The total water turbidity increased several times to more than 10-fold of that before the typhoon.

MATERIALS AND METHODS

A SD204 CTD (SAIV), which was lowered and raised at a rate of ~1.0 m s^{-1}, was used to continuously record water temperature, salinity, depth, turbidity and chl *a* (fluorometer sensor; SEAPOINT) data throughout the water column. The fluorometer

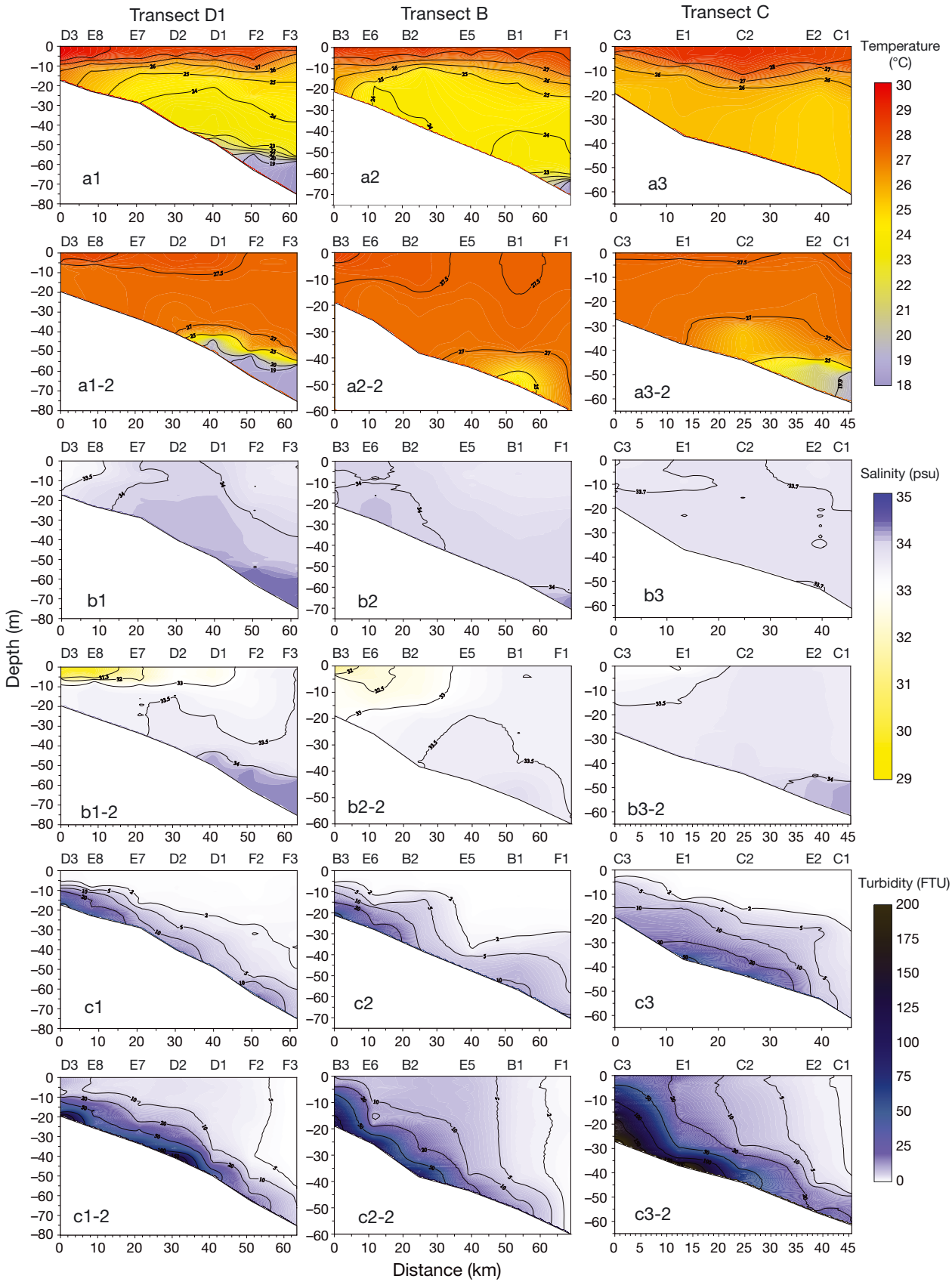

Fig. 2. (a) Temperature, (b) salinity and (c) turbidity distributions along Transects (1) D1, (2) B and (3) C before the typhoon and (1-2) D1, (2-2) B and (3-2) C after the typhoon

had a detection range of 0 to 10 mg m^{-3} and a sampling frequency of 1 s^{-1}.

The surface chl *a* and SST remote sensing data were obtained from Aqua-MODIS level 2 data (http://oceancolor.gsfc.nasa.gov/cgi/browse.pl?sen=am) from 31 July, 13 August and 16 August 2009. Due to the heavy cloud cover during the typhoon, the quality of the remote sensing images was so low that we only obtained 3 good-quality images. The data, which had a spatial resolution of 1.1 × 1.1 km, were processed by a SeaDAS 4.9 Mercator projection to produce level 3 data for the Zhejiang-Fujian coastal sea area (25 to 30° N latitude, 120 to 125° E longitude) (http://seadas.gsfc.nasa.gov/doc/tutorial/sds_tut2.html).

RESULTS

Distribution of fluorescent chl *a* before and after Typhoon Morakot

The distribution of fluorescent chl *a* along Transects D1, B and C in the pre- and post-Morakot surveys is shown in Fig. 2. Before the typhoon, the chl *a* concentration was between 0.2 and 9.0 mg m^{-3} and higher (generally >0.7 mg m^{-3}) in the coastal area, where the water depth was <25 m. In the water column where the water depth was >25 m, the chl *a* concentration was low at the bottom and the surface layer but high in the middle layer. The high-concentration zone appeared below the thermocline (at ~10 m depth). Chl *a* concentration generally increased from the northern transect (D1) to the southern transect (C) and markedly decreased away from the coast. Transects B and C displayed a discontinuous pattern; the middle water mass was rich in chl *a* but was divided in the central transect (Fig. 3a–c).

After the passage of the typhoon, the chl *a* concentration was generally maintained at low levels, with values <0.5 mg m^{-3} in most of the study area. The upper 10 m layer of the coastal water along Transects D1 and B contained high chl *a*, which gradually decreased from Transect D1 to Transect B (Fig. 3d,e). On Transect C, the chl *a* concentration was relatively high around Stns E2 and C1, where the water was >50 m deep, and gradually decreased toward the coast (Fig. 3f). From Transects D1 to C, the chl *a* concentration in the deep-water areas (>40 m deep) generally increased (bordered by the 0.5 mg m^{-3} contour), and the extension of relatively high chl *a* (>0.5 mg m^{-3}) to the coast gradually increased too. Along Transect C, the maximum chl *a* concentration was >0.9 mg m^{-3} (even higher than normal conditions) (Fig. 3c), and the water column with chl *a* concentration >0.5 mg m^{-3} could extend ~35 km

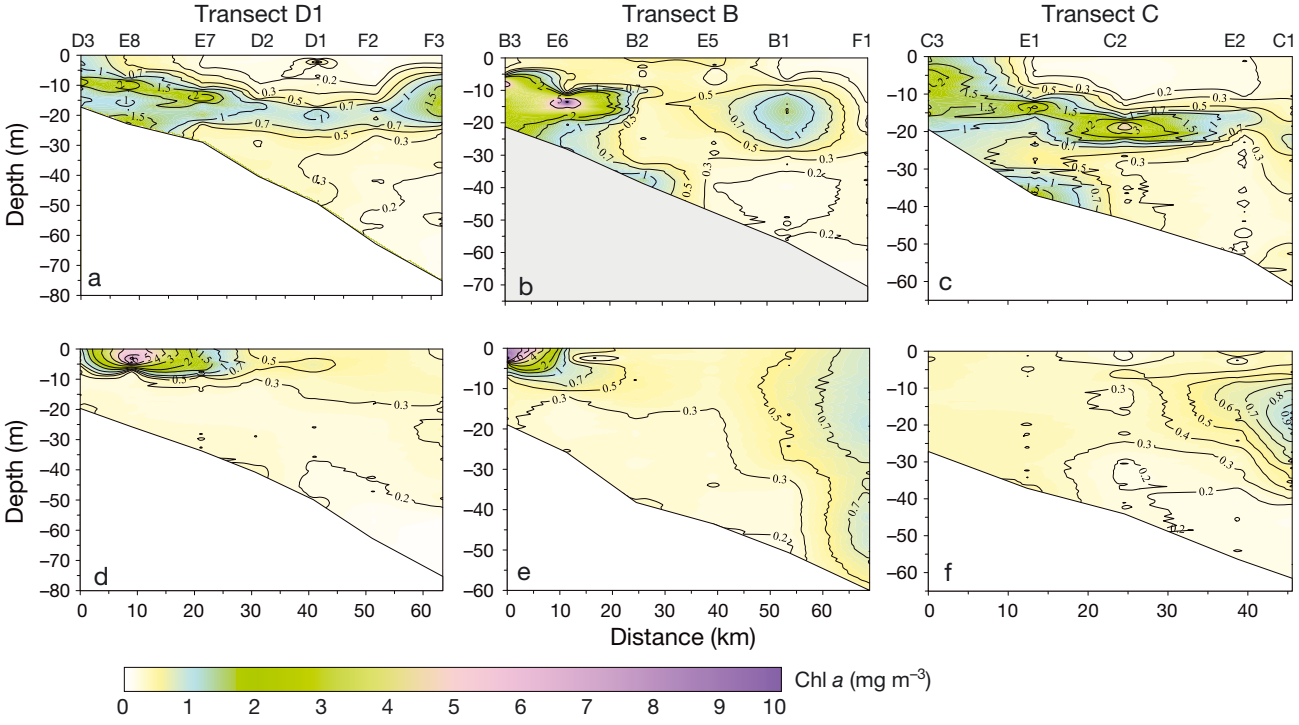

Fig. 3. Chl *a* distribution along Transects (a,d) D1, (b,e) B and (c,f) C (a–c) before and (d–f) after the typhoon

away from the coast (Fig. 3f). Along Transect B, the maximum chl *a* concentration was >0.7 mg m^{-3}, and the water column with chl *a* concentration >0.5 mg m^{-3} could extend ~55 km away from the coast (Fig. 3e). In contrast, the chl *a* concentration was <0.5 mg m^{-3} below the 40 m depth along Transect D1 (Fig. 3d).

Comparison of the chl *a* distribution before and after the typhoon revealed several patterns. First, before the typhoon, chl *a* was primarily present in the coastal shallow water and the euphotic zone (below the thermocline). After the landfall of Typhoon Morakot, increased water mixing induced the disappearance of the thermocline (Fig. 2), and the chl *a* concentration was dramatically decreased in most of the water column. Second, after landfall, the increase in land runoff led to the formation of a wedge of low-salinity water in the coastal surface water and introduced a great deal of terrigenous nutrients into the system (Fig. 2), which resulted in a rapid increase in chl *a* concentration in the low-salinity water. Third, in the water column with water depth >40 m, the chl *a* concentration, higher than normal conditions (Fig. 3c,f), gradually increased from the north to the south (Fig. 3d–f).

Distributions of chl *a* and SST in remote sensing images

Heavy cloud cover was associated with the routing and landing of the typhoon, which compromise remote sensing data. Our screening and processing generated 3 images from available remote sensing images for the study area and surroundings, which were on 31 July (normal, pre-typhoon condition), 13 August (close to the timing of the second field survey, i.e. the typhoon-active period condition) and 16 August (post-typhoon condition; Fig. 4). Although the quality of the second image was poor due to the direct impact of Typhoon Morakot, particularly in the study area, the remote sensing data are in good agreement with the field data. The general pattern of the chl *a* distribution could be better revealed through combination of the 2 datasets.

Despite large areas of cloud cover, several patterns of chl *a* distribution could still be observed in the study area. First, under normal, pre-typhoon conditions, an increase in water depth was correlated with the gradual reduction of chl *a* at the sea surface. The coastal area had a chl *a* concentration of ~1 mg m^{-3} (Fig. 4a), which was almost equal to the value

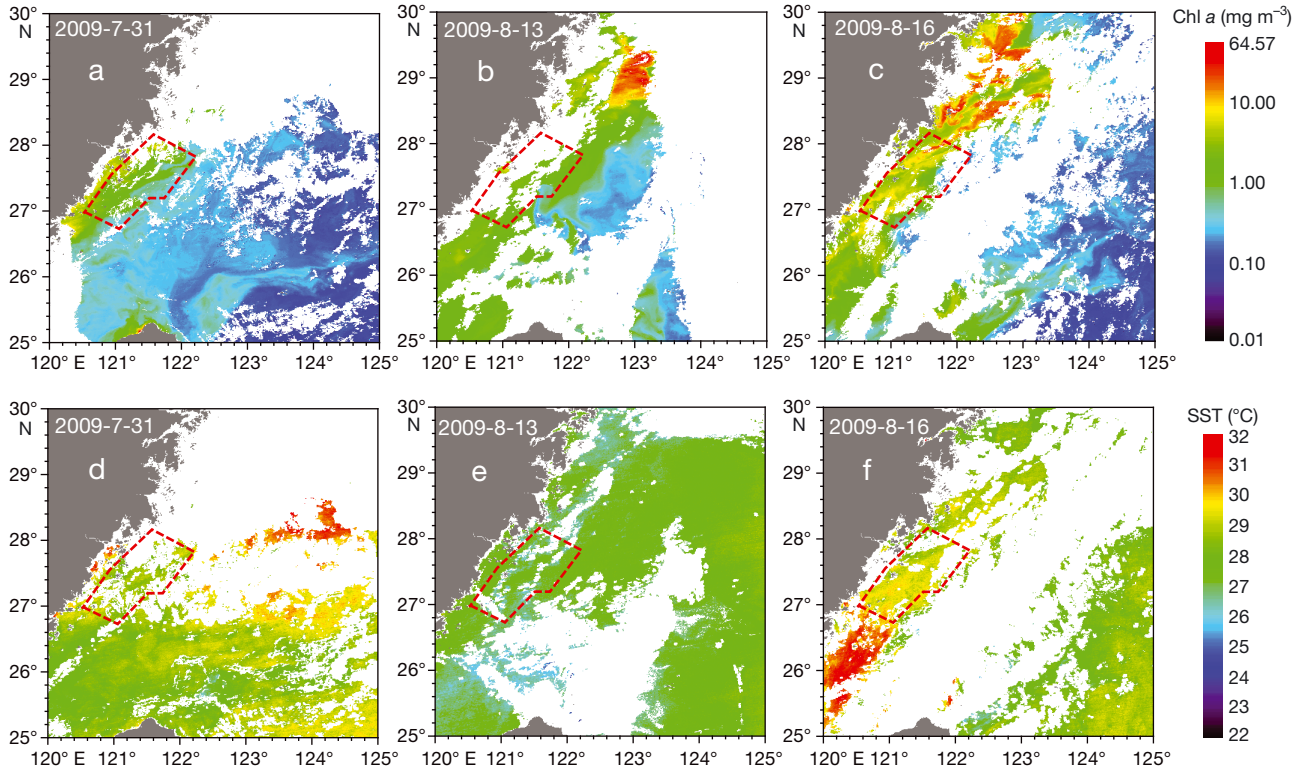

Fig. 4. (a–c) Chl *a* and (d–f) sea surface temperature (SST) distributions on 31 July, 13 August and 16 August 2009. The red dashed box indicates the field survey zone. Data were taken from http://oceancolor.gsfc.nasa.gov/

obtained through the field survey (Fig. 3a–c). Second, the coastal area chl *a* levels were similar under the pre-typhoon condition and the typhoon-active period condition; however, in the southern and eastern areas, where the typhoon effects occurred first, the chl *a* concentration was considerably increased under the typhoon-active period condition. In Hangzhou Bay, located in the north of the study area, the increase in runoff contributed to a dramatic increase in the chl *a* concentration, with a maximum value of >10 mg m^{-3} (Fig. 4b), which agreed with the value obtained from field observations (Fig. 3d,e). Third, during post-typhoon conditions, the chl *a* concentration clearly increased compared to that during normal, pre-typhoon conditions. This pattern was more pronounced in the coastal area, where the maximum chl *a* concentration was >10 mg m^{-3}. As the runoff diffused southward, the high chl *a* concentration water also spread southward, reaching the farthest point in the central study area (Fig. 4f).

Several features can be observed from the SST distribution in Fig. 4. First, under normal conditions, the water mass has a relatively high temperature, which is generally >28°C and gradually decreases from the coast to the deep water (Fig. 4d). Second, after passage of the typhoon, the SST was lower than the normal condition and displayed a relatively uniform distribution, showing little spatial variation (Fig. 4e). Third, as the influence of the typhoon reached its termination, the SST again showed a marked increase and a gradually reducing trend from southwest to northeast; this trend is similar to that under normal conditions (Fig. 4d,f). The patterns of the SST distribution also show good agreement with the field measurements (Fig. 2).

DISCUSSION

Typhoon-induced chl *a* variations and temporal lags

Field investigations revealed that the vertical chl *a* distributions developed in 2 stages: the pre-typhoon (normal) and typhoon-active period conditions, respectively. Remote sensing, comparatively, provided 3 stages of development for the surface chl *a* and SST distributions: the pre-typhoon (normal), typhoon-active period and post-typhoon conditions. The combination of the 2 datasets more comprehensively reflects the impact of the typhoon on the chl *a* distribution than either dataset alone. The following analyses of the variation in chl *a* during the first 2 stages were primarily based on the field surveys because of clouds covering a large portion of study area during the typhoon. However, the remote sensing image on 16 August 2009 provided a valuable demonstration of the third stage.

Chl *a* is generally enriched in the euphotic zone below the thermocline, and its growth is mainly influenced by temperature, light intensity and nutrients in the water (Suchint & Puntip 2000). In coastal and upwelling areas, where nutrient-rich water is available, phytoplankton undergo robust growth and therefore boost the chl *a* concentration (Estrada & Blasco 1985). Typhoon processes can also significantly enhance the chl *a* concentration due to several mechanisms, as indicated in previous studies (Lin et al. 2003, Babin et al. 2004, Zheng & Tang 2007, Huang et al. 2011). First, the strong winds promote vertical water mixing and cause strong upwelling (or downwelling). These 2 consequential factors together propel nutrient-rich water from the lower water column to the euphotic zone, thereby initiating a phytoplankton bloom and increasing the marine primary productivity (Lin et al. 2003, Babin et al. 2004, Zheng & Tang 2007). Second, typhoon-induced heavy precipitation increases the material flux (e.g. terrigenous fresh water, particles, nutrients and nutrient-rich aerosols), which can also stimulate phytoplankton growth and enhance the marine primary productivity (Huang et al. 2011). In addition, the stratification and thermocline are interrupted after the passage of the typhoon, resulting in more active ocean–atmosphere material and energy exchanges and thereby increasing the dissolved oxygen that boosts phytoplankton growth in water (Dickey et al. 1998, Souza et al. 2001, Lin et al. 2003). Meanwhile, as the water mixing intensifies, the thermocline is altered and the surface temperature significantly decreases, which is more suitable for the growth of organisms. All of these factors can lead to the proliferation of marine organisms and thus an increase in chl *a* concentration.

An increase in dissolved oxygen and nutrients does not lead to an immediate increase in chl *a* concentration because it may take days for the nutrients to be taken up by the organisms. Moreover, the growth of marine organisms is clearly affected by light, which is markedly reduced during a typhoon event as a result of cloud cover and increased water turbidity. Hence, typhoon-induced chl *a* increases that are mediated by the growth of aquatic organisms display a time-lag effect (Babin et al. 2004), which is determined by the degree and intensity of the typhoon process and the biological activity cycles.

Throughout the second survey, the weather was unfavorable, and the coastal area was cloudy and windy, with wind speeds >13.0 m s^{-1} (Ocean Monitoring and Forecasting Center of Zhejiang Providence, www.zjhy.net.cn). The growth of phytoplankton was limited by the weak light (due to the cloud cover and turbid water caused by the increased particle supply and sediment resuspension during the typhoon), and consequently, the concentration of chl *a* in most of the water column decreased during the second survey. In contrast, in the coastal area, the concentration of chl *a* increased in the surface water layer and was accompanied by a halocline that appeared at ~10 m depth (Fig. 2) due to the abundant terrigenous materials (e.g. fresh water, particles and nutrients) supplied from runoff during the typhoon (Fig. 3d,e).

As the typhoon migrated northward, the areas earliest influenced by the typhoon were first to experience the improved conditions of phytoplankton growth, which were followed by an increase in chl *a* concentration. In the second survey, the concentration of chl *a* in the deep water column (>40 m depth) along Transect C, the first place to recover from the impacts of the typhoon, was even higher than that before the typhoon. This is likely attributable to the effects of water mixing and the upwelling of nutrient-rich bottom water (Fig. 3f).

With the settling of resuspended particles, the clearing of cloud cover and the normalization of light conditions after the passage of the typhoon, the phytoplankton bloomed as the opposing factors disappeared, and increases in nutrients and dissolved oxygen drove an increase in chl *a* (Fig. 4c). Due to the time delay involved with biogeochemical processes, such as nutrient absorption and then a phytoplankton bloom, the peak of the chl *a* concentration occurred several days after the passage of the typhoon. Without a time series of data, the exact delay time cannot be obtained. However, according to the high chl *a* concentration that appeared in the deep water column along Transect C (Fig. 3f) and the distributions of surface chl *a* in the remote sensing images (Fig. 4), a reasonable conclusion can be drawn that the peak chl *a* concentration most likely occurred ~4 to 7 d after the passage of Typhoon Morakot, which was similar to that found in previous studies (e.g. Babin et al. 2004).

Chl *a* evolution model initiated by typhoon processes in the near-shore area

The temporal and spatial variations in chl *a* distribution caused by typhoon processes vary significantly with water depth. In the coastal area, the supplies of terrigenous materials and nutrient particles were generally richer than those in the deep water, and the impacts of the typhoon were more complicated because the typhoon-induced cyclonic wind stress easily stirred the sediment and induced significant resuspension. The impact of typhoon processes on chl *a* distribution is more complicated in the coastal area than in deep water (Zheng & Tang 2007). Based on the above analysis, a conceptual model with 3 stages is proposed concerning the temporal evolution of chl *a* during typhoon processes in the inner shelf area (including coastal areas) (Fig. 5).

Stage 1: Normal (pre-typhoon) condition (Fig. 5a). There is a stable supply of terrigenous material and a normal light intensity at the sea surface. The water column is stratified and has a distinct thermocline (Figs. 2, 3a–c & 4a,d). The sediment suspension is primarily concentrated at the bottom of the water column (Fig. 2). In this stage, chl *a* is mostly distributed in the coastal shallow water and in the euphotic zone below the thermocline.

Stage 2: Typhoon-active period condition (Fig. 5b). This stage covers a couple of days before and after the typhoon arrives. The terrigenous material supply increases and forms a wedge of low-salinity water in the coastal area (Fig. 2). The upper water layer (<40 m depth) is well-mixed, the stratification and thermocline are interrupted, and large amounts of sediments are re-suspended and enter the water column due to the typhoon-induced water mixing and upwelling (Fig. 2). The light intensity and transmittance both decline due to cloud cover and high turbidity. In this stage, the chl *a* concentration decreases in most areas (Figs. 3d–f & 4b,e) but may be relatively high in the terrigenous water wedge due to the nutrient-rich fresh water supply.

Stage 3: Post-typhoon condition (Fig. 5c). This stage is ~4 to 7 d after the typhoon arrives. As the direct influence of the typhoon weakens and gradually disappears, the factors opposing phytoplankton growth disappear, light intensity recovers, and aquatic particles gradually settle, and the increased nutrient and dissolved oxygen supply due to the typhoon lead to a rapid proliferation of phytoplankton and an increase in chl *a* concentration (Dickey et al. 1998, Souza et al. 2001, Lin et al. 2003).

As the marine environment gradually recovers, the water structure and chl *a* concentration return to their normal state. The water structure, in terms of temperature, salinity and turbidity distributions, recovers prior to the chl *a* distribution due to the time delay involved with biogeochemical processes such

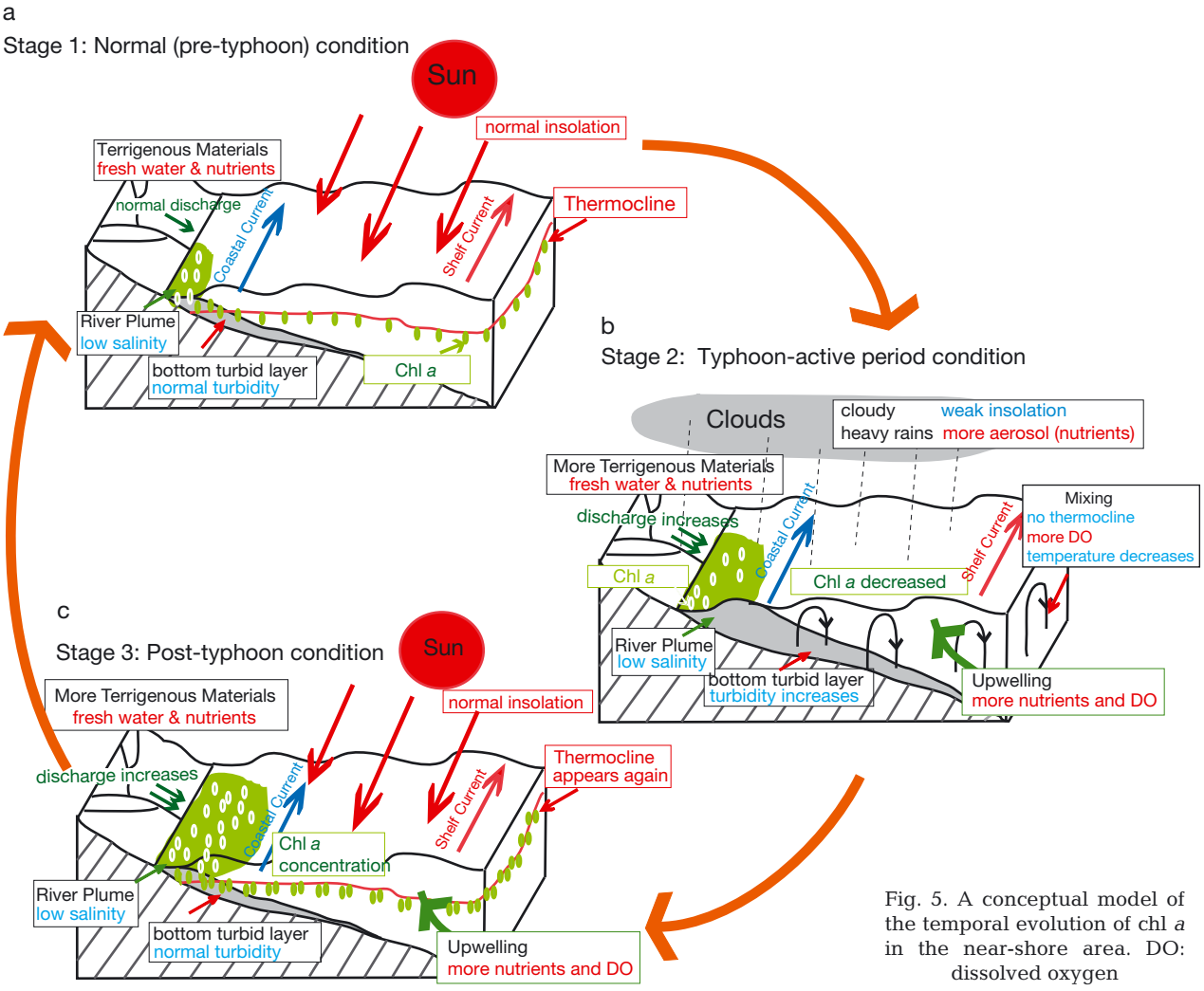

Fig. 5. A conceptual model of the temporal evolution of chl *a* in the near-shore area. DO: dissolved oxygen

as nutrient absorption and then phytoplankton blooming (Zheng & Tang 2007).

CONCLUSION

In situ cruise and satellite remote sensing data were combined to study the impact of Typhoon Morakot on the chl *a* distribution on the inner shelf of the East China Sea. A conceptual model was proposed concerning the temporal evolution of chl *a* in the inner shelf area. Three conclusions are drawn based on the study results and discussions.

(1) Under typhoon conditions, the concentration of chl *a* decreases primarily due to the typhoon-induced absence of light and the high water turbidity. However, in the coastal surface water layer, the concentration of chl *a* increases due to the sufficient supply of terrigenous particles and fresh water during the typhoon.

(2) Under post-typhoon conditions, the concentration of chl *a* gradually increases because the factors opposing phytoplankton growth disappear and nutrient and dissolved oxygen supply increase due to the typhoon process.

(3) In general, typhoon processes can significantly boost chl *a* concentration and marine primary productivity, but this impact shows a temporal lag of ~4 to 7 d in the inner shelf area.

Acknowledgements. We thank all of the investigators for their help in collecting samples and data during the 2 surveys. The remote sensing data were calculated by Dr. Y. H. Li and J. Li of Xiamen University. This work was supported by the National Science Foundation of China (NSFC, grant nos. 40806024, 41276059 and 41076035) and the Scientific Research Foundation of the Third Institute of Oceanography, SOA (grant no. TIO2008004). This manuscript benefited from comments and suggestions of Katherine Richardson and 3 anonymous reviewers.

LITERATURE CITED

Babin SM, Carton JA, Dickey TD, Wiggert JD (2004) Satellite evidence of hurricane-induced phytoplankton blooms in an oceanic desert. J Geophys Res 109:C03043, doi:10.1029/2003JC001938

Bian CW, Jiang WS, Song DH (2010) Terrigenous transportation to the Okinawa Trough and the influence of typhoons on suspended sediment concentration. Cont Shelf Res 30:1189–1199

Byju P, Kumar SP (2011) Physical and biological response of the Arabian Sea to tropical cyclone Phyan and its implications. Mar Environ Res 71:325–330

Chang GC, Dickey TD, Williams AJ III (2001) Sediment resuspension over a continental shelf during Hurricanes Edouard and Hortense. J Geophys Res 106:9517–9531

Chen CTA, Liu CT, Chuang WS, Yang YJ, Shiah FK, Tang TY, Chuang SW (2003) Enhanced buoyancy and hence upwelling of subsurface Kuroshio waters after a typhoon in the southern East China Sea. J Mar Syst 42:65–79

Davis A, Yan XH (2004) Hurricane forcing on chlorophyll-a concentration off the northeast coast of the U.S. Geophys Res Lett 31:L17304, doi:10.1029/2004GL020668

Dickey T, Frye D, McNeil J, Manov D and others (1998) Upper-ocean temperature response to Hurricane Felix as measured by the Bermuda testbed mooring. Mon Weather Rev 126:1195–1201

Eliot M, Pattiaratchi C (2010) Remote forcing of water levels by tropical cyclones in southwest Australia. Cont Shelf Res 30:1549–1561

Estrada M, Blasco D (1985) Phytoplankton assemblages in coastal upwelling areas. In: Bas C, Margalef R, Rubias P (eds) International Symposium of Upwelling of W. Africa, Vol 1. Instituto de Investigationes Pesqueras, Barcelona, p 379–402

Goñi MA, Gordon ES, Monacci NM, Clinton R, Gisewhite R, Allison MA, Kineke G (2006) The effect of Hurricane Lili on the distribution of organic matter along the inner Louisiana shelf (Gulf of Mexico, USA). Cont Shelf Res 26: 2260–2280

Herbeck LS, Unger D, Krumme U, Liu SM, Jennerjahn TC (2011) Typhoon-induced precipitation impact on nutrient and suspended matter dynamics of a tropical estuary affected by human activities in Hainan, China. Estuar Coast Shelf Sci 93:375–388

Hu DX, Yang ZS (eds) (2001) The key process of marine flux in the East China Sea. Ocean Press, Beijing (in Chinese)

Huang W, Mukherjee D, Chen SS (2011) Assessment of Hurricane Ivan impact on chlorophyll-a in Pensacola Bay by MODIS 250 m remote sensing. Mar Pollut Bull 62: 490–498

Li M, Zhong LJ, Boicourt WC, Zhang SL, Zhang DL (2007) Hurricane-induced destratification and restratification in a partially-mixed estuary. J Mar Res 65:169–192

Li YH, Wang AJ, Qiao L, Fang JY, Chen J (2012) The impact of Typhoon Morakot on the modern sedimentary environment of the mud deposition center off the Zhejiang-Fujian coast, China. Cont Shelf Res 37(C):92–100

Lin II, Liu WT, Wu CC, Chiang JCH, Sui CH (2003) Satellite observations of modulation of surface winds by typhoon-induced upper ocean cooling. Geophys Res Lett 30:1131, doi:10.1029/2002GL015674

Liu JL, Cai SQ, Wang SG (2011) Observations of strong near-bottom current after the passage of Typhoon Pabuk in the South China Sea. J Mar Syst 87:102–108

Liu JP, Li AC, Xu KH, Velozzi DM, Yang ZS, Milliman JD, DeMaster DJ (2006) Sedimentary features of the Yangtze River-derived along-shelf clinoform deposit in the East China Sea. Cont Shelf Res 26:2141–2156

Liu JP, Xu KH, Li AC, Milliman JD, Velozzi DM, Xiao SB, Yang ZS (2007) Flux and fate of Yangtze River sediment delivered to the East China Sea. Geomorphology 85: 208–224

Liu XM, Wang MH, Shi W (2009) A study of a Hurricane Katrina-induced phytoplankton bloom using satellite observations and model simulations. J Geophys Res 114: C03023, doi:10.1029/2008JC004934

McKinnon AD, Meekan MG, Carleton JH, Furnas MJ, Duggan S, Skirving W (2003) Rapid changes in shelf waters and pelagic communities on the southern Northwest Shelf, Australia, following a tropical cyclone. Cont Shelf Res 23:93–111

Milliman JD, Lin SW, Kao SJ, Liu JP, Liu CS, Chiu JK, Lin YC (2007) Short term changes in seafloor character due to flood-derived hyperpycnal discharge: typhoon Mindulle, Taiwan, July 2004. Geology 35:779–782

NMCCMA (National Meteorological Center, China Meteorological Administration) (2009) Pathway of typhoon. China Meteorological Administration, Beijing. Available at http://map.weather.gov.cn/ (in Chinese)

Price JF (1981) Upper ocean response to a hurricane. J Phys Oceanogr 11:153–175

Rao AD, Joshi M, Jain I, Ravichandran M (2010) Response of subsurface waters in the eastern Arabian Sea to tropical cyclones. Estuar Coast Shelf Sci 89:267–276

Shiah FK, Chung SW, Kao SJ, Gong GC, Liu KK (2000) Biological and hydrographical responses to tropical cyclones (typhoons) in the continental shelf of the Taiwan Strait. Cont Shelf Res 20:2029–2044

Souza AJ, Dickey TD, Chang GC (2001) Modeling water column structure and suspended particulate matter on the Middle Atlantic continental shelf during the passages of Hurricanes Edouard and Hortense. J Mar Res 59: 1021–1045

Su JL (ed) (2005) The oceanography in the Chinese margin sea. Ocean Press, Beijing (in Chinese)

Suchint D, Puntip W (2000) Sub-thermoline chlorophyll maximum in the South China Sea. Proceeding of the SEAFDEC seminar on fishery resources in the South China Sea Area IV: Vietnamese water. Southeast Asian Fisheries Development Center, Bangkok, p 1–17

Walker ND, Leben RR, Balasubramanian S (2005) Hurricane-forced upwelling and chlorophyll *a* enhancement within cold-core cyclones in the Gulf of Mexico. Geophys Res Lett 32:L18610, doi:10.1029/2005GL023716

Xu KH, Li AC, Liu JP, Milliman JD and others (2012) Provenance, structure, and formation of the mud wedge along inner continental shelf of the East China Sea: a synthesis of the Yangtze dispersal system. Mar Geol 291-294: 176–191

Zheng GM, Tang DL (2007) Offshore and nearshore chlorophyll increases induced by typhoon winds and subsequent terrestrial rainwater runoff. Mar Ecol Prog Ser 333: 61–74

Zheng ZW, Ho CR, Zheng QA, Kuo NJ, Lo YT (2010) Satellite observation and model simulation of upper ocean biophysical response to Super Typhoon Nakri. Cont Shelf Res 30:1450–1457

Editorial responsibility: Katherine Richardson, Copenhagen, Denmark

Submitted: April 23, 2012; Accepted: December 12, 2012
Proofs received from author(s): May 4, 2013